International Journal of Nanomedicine

Dovepress
Taylor & Francis Group

Open Access Full Text Article

ORIGINAL RESEARCH

pH-Sensitive Long-Circulating Nanoliposomes with CU1 for Effective Against Lung Cancer

Yuqian Pu[1–3,*], Yongqiang Jiang[1–3,*], Xinya Li[1–3,*], Ke Li[1–3], Qiong Zhang[1–3], Rong Zhang[4], Jiyuan Yuan[2], Chao Pi[1,3], Mei Hu[3], Yumeng Wei[3], Ling Zhao[2,3]

[1]Key Laboratory of Medical Electrophysiology, Ministry of Education, School of Pharmacy, Southwest Medical University, Luzhou, Sichuan, 646000, People's Republic of China; [2]Luzhou Key Laboratory of Traditional Chinese Medicine for Chronic Diseases Jointly Built by Sichuan and Chongqing, The Affiliated Traditional Chinese Medicine Hospital, Southwest Medical University, Luzhou, Sichuan, 646000, People's Republic of China; [3]Central Nervous System Product Research and Development Key Laboratory of Sichuan Province, School of Pharmacy, Southwest Medical University, Luzhou, Sichuan, 646000, People's Republic of China; [4]Department of Medical Statistics and Epidemiology, School of Public Health, Southwest Medical University, Luzhou, Sichuan, People's Republic of China

*These authors contributed equally to this work

Correspondence: Yumeng Wei, Central Nervous System Product Research and Development Key Laboratory of Sichuan Province, School of Pharmacy, Southwest Medical University, No. 1, Section 1, Xianglin Road, Longmatan District, Luzhou, Sichuan, 646000, People's Republic of China, Tel/Fax +86 830-3162291, Email weiyumeng@swmu.edu.cn; Ling Zhao, Luzhou Key Laboratory of Traditional Chinese Medicine for Chronic Diseases Jointly Built by Sichuan and Chongqing, The Affiliated Traditional Chinese Medicine Hospital, Southwest Medical University, No. 182, Chunhui Road, Longmatan District, Luzhou, Sichuan, 646000, People's Republic of China, Tel/Fax +86 830-2681630, Email zhaol@swmu.edu.cn

Introduction: To address the poor water solubility and low bioavailability of the curcumin derivative CU1, this study constructed a long-circulating pH-sensitive nanoliposome (CU1-LCpHL) as its delivery system.

Methods: The physicochemical properties, stability, and anti-lung cancer efficacy of CU1-LCpHL were systematically evaluated, including in vitro cellular assays (cellular uptake, apoptosis, proliferation, and migration), in vivo pharmacokinetics and pharmacodynamics, mechanistic studies, and immunohistochemical analysis.

Results: CU1-LCpHL presented a spherical morphology with uniform particle size. Its lyophilized powder remained stable for at least three months at 25°C and exhibited sustained-release characteristics. In vitro experiments demonstrated that, compared to free curcumin (CU), free CU1, and long-circulating stable nanoliposomes (CU1-LSLN), CU1-LCpHL promoted more efficient cellular uptake, induced apoptosis, and significantly inhibited the proliferation and migration of lung cancer cells. Pharmacokinetic studies revealed that the area under the curve (AUC_{0-t}) of CU1-LCpHL was 9.52-fold and 9.47-fold higher than that of CU and CU1, respectively, while its mean residence time (MRT_{0-t}) was 3.37-fold and 7.69-fold longer, respectively. In vivo pharmacodynamic results indicated that the tumor-inhibition rate of CU1-LCpHL was 2.42-, 2.17-, and 1.37-fold higher than those of CU, CU1, and CU1-LSLN, respectively, with no significant organ toxicity or hemolysis observed. Mechanistic studies showed that CU1-LCpHL significantly upregulated Caspase-3, Caspase-9, and Bax, while downregulating the p-AKT/AKT ratio and Bcl-2 levels. Immunohistochemical analysis further confirmed that CU1-LCpHL markedly reduced the positive expression of Ki67, CD34, and VEGFR2, outperforming all other treatment groups.

Conclusion: CU1-LCpHL significantly enhances the delivery efficiency and antitumor efficacy of CU1, representing a promising nano-drug delivery system for lung cancer therapy.

Keywords: curcumin derivative, long-circulating pH-sensitive nanoliposomes, lung cancer efficacy, pharmacokinetics, mechanism

Introduction

According to the data released by the International Agency for Research on Cancer (IARC) in 2022, there were approximately 20 million new cancer cases and a staggering 9.7 million cancer deaths worldwide. Among these, lung cancer accounted for 1.8 million deaths, posing a severe threat to human life and health.[1,2] The insidious nature of early-stage lung cancer symptoms often leads to diagnosis at advanced stages, causing patients to miss the optimal window for surgical intervention. Consequently, chemotherapy undoubtedly holds a crucial position in clinical management.

https://doi.org/10.2147/IJN.S588259
Received: 11 December 2025
Accepted: 5 March 2026
Published: 16 March 2026

Graphical Abstract

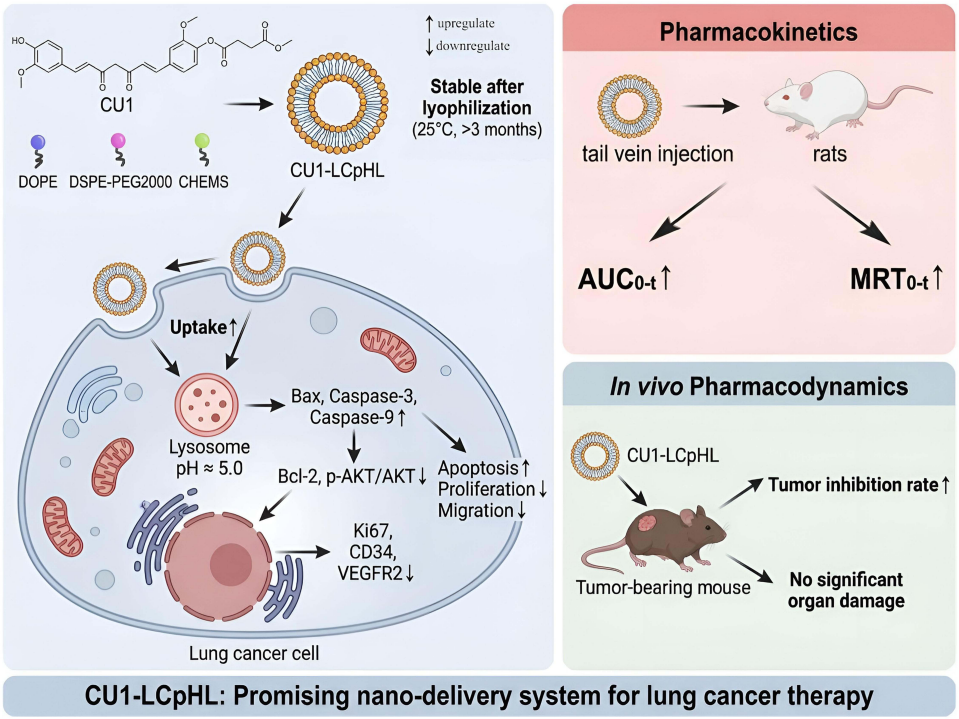

However, conventional chemotherapeutic agents are often plagued by limited efficacy and significant toxic side effects, failing to substantially improve patients' quality of life.[3–5] Therefore, the development of novel anti-lung cancer agents and delivery systems with high efficacy and low toxicity is urgently needed.

In recent years, natural product monomers have attracted significant attention in cancer therapy due to their wide availability, diverse biological activities, and relative safety.[6,7] Curcumin (CU), the primary active constituent of the traditional Chinese medicine turmeric, has been extensively documented in pharmacological studies to exert anti-lung cancer effects through multiple pathways. These include inhibiting the activity of protein kinases (eg, MAPK, Akt), modulating the expression of apoptosis-related proteins (eg, Bcl-2, Bax), and downregulating pro-angiogenic factors such as vascular endothelial growth factor (VEGF).[3,8] Clinical studies have also indicated that high-dose oral administration of CU (eg, 8 g daily) exhibits biological activity in cancer chemoprevention without observable significant toxicity,[9] suggesting CU as a promising anti-lung cancer candidate with good safety. Nonetheless, its clinical translation and application are severely hampered by inherent drawbacks, including instability, poor aqueous solubility, and low oral bioavailability.[10–12]

To overcome the limitations of CU, our research team previously designed and synthesized a novel derivative, CU1, by modifying the phenolic hydroxyl groups in the CU structure. This derivative demonstrated significant improvements over CU in terms of stability, cell permeability, and in vitro anti-lung cancer activity.[13] To further enhance its in vivo delivery efficiency, the team developed a non-pH-sensitive long-circulating nanoliposome (CU1-LSLN) that moderately prolonged the blood circulation time of CU1. Yet, its anti-tumor efficacy remained suboptimal.[13] Solid tumor tissues often develop a unique acidic microenvironment (pH 5.0–6.5) due to abnormal metabolism,[14,15] a characteristic closely associated with tumor cell proliferation, invasion, and migration.[16,17] Exploiting this pathological feature, the design of intelligent stimuli-responsive drug delivery systems has become a research hotspot. pH-sensitive liposomes can overcome traditional drug-delivery bottlenecks and enhance targeted therapy efficacy, demonstrating significant translational

clinical value. Conventional liposomes are prone to clearance by the reticuloendothelial system and exhibit short half-lives. Extended-circulation liposomes achieve prolonged in vivo stability through surface modification, reducing systemic exposure and adverse effects. pH-sensitive liposomes maintain stability and circulation under physiological pH conditions. Within the acidic tumor microenvironment, they undergo structural transformation, enabling specific drug accumulation and rapid release at the lesion site. This enhances tumor tissue permeability and cellular uptake efficiency, ultimately improving the therapeutic index while reducing systemic toxicity.[18–21] Among these, lipid bilayer structures composed of dioleoylphosphatidylethanolamine (DOPE) and cholesteryl hemisuccinate (CHEMS) are stable under physiological conditions. In an acidic environment, the protonation of CHEMS disrupts membrane stability, triggering the release of the encapsulated drug.[22–24] Furthermore, the incorporation of polyethylene glycolated phospholipids (eg, DSPE-PEG2000) can enhance passive targeting to tumor tissue via the enhanced permeability and retention (EPR) effect.[24,25] This combination of materials exhibits no significant cytotoxicity.[26]

Therefore, to further optimize the pharmacokinetic profile and enhance the anti-lung cancer efficacy of CU1, this study aims to construct a novel pH-responsive acid-sensitive nanoliposome (CU1-LCpHL). The research will first focus on optimizing the formulation process and systematically characterizing the constructed liposomes. Subsequently, the cellular uptake, apoptosis induction, and effects on the proliferation and migration of lung cancer cells by CU1-LCpHL will be evaluated in vitro. In animal models, our team will comprehensively investigate its pharmacokinetic behavior, anti-lung cancer pharmacodynamics, and preliminary safety. Finally, integrating network pharmacology predictions and employing techniques such as Western blot and immunohistochemistry, the study will preliminarily elucidate the underlying molecular mechanisms at both cellular and animal levels. This work aims to provide experimental evidence and a theoretical foundation for the development of targeted lung cancer therapies and novel formulations based on natural active components.

Materials and Methods

Chemicals, Cell Lines, and Animals

CU1 was synthesized by the Central Nervous System Product Research and Development Key Laboratory of Sichuan Province, Southwest Medical University. DSPE-PEG2000 was supplied by Lipoid GmbH (Ludwigshafen, Germany). DOPE was purchased from Corden Pharma (Liestal, Switzerland). CHEMS was obtained from Sigma-Aldrich (St. Louis, MO, USA). The human non-small cell lung cancer (NSCLC) A549 cell line was provided by the Cell Bank of the Chinese Academy of Sciences (Shanghai, China). Cells were cultured in high-glucose Dulbecco's Modified Eagle's Medium (DMEM) (Gibco, Thermo Fisher Scientific, Inc., USA) supplemented with 10% fetal bovine serum (FBS) (Hyclone, Utah, USA). The Annexin V-FITC apoptosis detection kit was purchased from Nanjing Jiancheng Bioengineering Institute (Nanjing, China).

The Synthesis of Long-Circulating pH-Sensitive Nanoliposome of CU1

Referring to previous literature,[25,27] a stable pH-sensitive lipid bilayer structure requires a specific molar ratio (6:4) of DOPE and CHEMS. Therefore, the final formulation of the liposomes was determined as DOPE: CHEMS: DSPE-PEG2000: CU1 (molar ratio) = 6:4:0.5:1. Specifically, the accurately weighed lipids (DOPE, CHEMS, DSPE-PEG2000) and the drug CU1 were co-dissolved in 1 mL of chloroform and mixed thoroughly. The solution was transferred into a 50 mL round-bottom flask. The flask was placed in a 37°Cwater bath, and the organic solvent was removed under reduced pressure using a rotary evaporator at 150 rpm until a uniform thin lipid film formed on the inner wall. The flask containing the lipid film was transferred to a desiccator and dried overnight at 37°C in the dark to completely remove residual solvent. The following day, 5 mL of pre-warmed phosphate-buffered saline (PBS, pH 7.2–7.4) at 37°C was added to the dried lipid film, and the mixture was gently swirled to facilitate complete dispersion of the lipid film. The resulting crude liposome suspension was then placed in an ice bath and sonicated using a probe sonicator (180 W, duty cycle: 4 s on/4 s off) for a total duration of 6 min to obtain a homogeneous nanoliposome dispersion (CU1-LCpHL), Using sucrose as a lyophilization protective agent for freeze-drying.

The Characterisation of Long-Circulating pH-Sensitive Nanoliposome of CU1 Particles

The synthesis method for CU1-LSLN has been previously reported.[25] An appropriate amount of CU1-LCpHL lyophilized powder or CU1-LCpHL dispersion was diluted in PBS (pH 7.2–7.4) to 0.2 mg/mL. The particle size, polydispersity index (PDI), and zeta potential (ZP) of CU1-LCpHL were measured using a Malvern Zetasizer Nano ZS (Malvern Instruments, UK).

Encapsulation Efficiency and Drug Loading

Free CU1 in the CU1-LCpHL dispersion precipitates during low-to-medium speed centrifugation.[28] A 100 μL aliquot of the CU1-LCpHL dispersion was centrifuged (8000 rpm, 3 min). Subsequently, 50 μL of the supernatant was transferred, mixed with 2 mL of acetonitrile under sonication, and centrifuged (8000 rpm, 10 min). The supernatant was analyzed by High-Performance Liquid Chromatography (HPLC) to determine the amount of encapsulated drug (W_1). Concurrently, 50 μL of the non-centrifuged CU1-LCpHL dispersion was accurately measured, mixed with 2 mL of acetonitrile, and processed identically to determine the total drug amount (W_0). The Encapsulation Efficiency (EE%) was calculated as (W_1/W_0) × 100%.A precise weight of the CU1-LCpHL lyophilized powder (C_0) was dissolved and diluted to an appropriate concentration with acetonitrile. The mixture was sonicated to disrupt the liposomes and centrifuged (8000 rpm, 10 min). The supernatant was analyzed by HPLC. The actual CU1 content (C_1) was calculated based on a standard curve and dilution factor, and the Drug Loading (DL%) was calculated as (C_1/C_0) × 100%.

The Electron Morphology and Stability

Ten microliters of the CU1-LCpHL dispersion were placed on a 200-mesh copper grid, stained with 10 μL of 1% (w/v) phosphotungstic acid for 1 min, air-dried, and then observed for particle morphology using a Hitachi H-7500 transmission electron microscope (Hitachi Ltd., Tokyo, Japan). Aliquots of the liposomal dispersion were stored at 4°C. Both the dispersion and lyophilized powder samples were also stored in a controlled environment chamber (25 ± 2 °C, 40 ± 5% relative humidity). Particle size, PDI, EE%, and DL% were measured at predetermined intervals to assess stability.

In vitro Release Study

The in vitro release profile of CU1 from CU1-LCpHL was determined using the dialysis bag method. Briefly, CU1 solution in acetonitrile and CU1-LCpHL dispersion were prepared at a concentration of 200 μg/mL (equivalent CU1). One milliliter of each preparation was sealed in dialysis bags (molecular weight cut-off: 8000–14,000 Da). The bags were then immersed in 200 mL of release medium (PBS, pH 5.5 or pH 7.4) maintained at 37 ± 0.5°C with stirring at 150 rpm. At predetermined time points (0.25, 0.5, 1, 1.5, 2, 4, 6, 8, 12, and 24 h), 2 mL samples were withdrawn from the release medium and immediately replaced with an equal volume of fresh, pre-warmed medium at the same pH to maintain sink conditions. The collected samples were filtered through a 0.22 μm membrane and analyzed for CU1 concentration by HPLC. Each condition was tested in triplicate.

Cellular Uptake

A549 cells were trypsinized, diluted with complete medium, and seeded into 6-well plates. Upon reaching the appropriate confluence, the medium was replaced with fresh complete medium containing 25 μM of CU, CU1, CU1-LSLN, or CU1-LCpHL, along with an untreated control group. After 3 h of incubation, the treatment medium was discarded, and the cells were washed twice with ice-cold PBS. The cells were then trypsinized, centrifuged, and the resulting pellet was resuspended in 0.5 mL of ice-cold PBS. Fluorescence intensity was measured using a flow cytometer.

Apoptosis Assay

A549 cells were trypsinized, diluted in complete medium, and seeded into 6-well plates at a density of 5×10^5 cells per well, then incubated for 24 h. The old medium was then replaced with fresh medium containing 25 μM of CU, CU1, CU1-LSLN, or CU1-LCpHL. After another 24 h, cells from each sample were collected. The cells were suspended in 1X

Annexin V binding buffer, then incubated with 5 μL of Annexin V-FITC and 5 μL of propidium iodide (PI) in the dark for 15 min. The cells were then analyzed by flow cytometry to identify and quantify apoptotic cells.

Cytotoxicity Study

Logarithmically growing A549 cells were uniformly seeded into 96-well plates at a density of 3000 cells per well and cultured for 24 h in a 5% CO_2 incubator at 37°C. After incubation, MTT solution (5 mg/mL) was added to each well, accounting for 10% of the total culture volume. Following an additional 4 h of incubation, the medium was carefully aspirated, and 100 μL of dimethyl sulfoxide (DMSO) was added to each well to dissolve the formazan crystals. The plate was then placed on an orbital shaker for 15 min. The optical density (OD) of each well was measured at 490 nm using a microplate reader. The cell inhibition rate was calculated as described previously.[29]

Cell Migration Assay

A549 cells were diluted with complete medium and seeded into 6-well plates. Cells (5×10^5 per well) were cultured for 24 h, then washed twice with PBS. A uniform scratch was made in each well using a 200 μL pipette tip. After washing twice with PBS to remove dislodged cells, images of the scratch area were taken under a microscope (0 h). The medium was then replaced with serum-free medium containing the same concentration (25 μM) of CU, CU1, CU1-LSLN, or CU1-LCpHL. The cells were cultured for an additional 24 h (37°C, 5% CO_2). Subsequently, the cells were washed twice with PBS, and images of the scratch area were taken again. The migration rate was calculated by comparing the differences in the wound width between the initial and final images.[30,31]

Pharmacokinetic Study

Based on the dosage determined in preliminary studies,[25] the equivalent dose of CU1 was set at 15 mg/kg. Healthy Sprague-Dawley rats (n=6 per group) were used. All rats were fasted for 8 h with free access to water before the experiment. The CU1 raw material solution, CU1-LSLN dispersion, and CU1-LCpHL dispersion, all containing an equivalent CU1 dose of 15 mg/kg, were administered via a single tail vein injection. Blood samples (approximately 0.3 mL) were collected from the tail vein at 3, 5, 10, 15, 30, 60, 120, 240, 480, 720, and 1440 min post-injection. The blood was placed in 1.5 mL centrifuge tubes pre-moistened with heparin sodium solution. Samples were centrifuged at 5000 rpm for 3 min at 4°C. The separated plasma was carefully transferred to new tubes and stored at −80 °C until analysis.Plasma samples were processed via protein precipitation and analyzed using a validated HPLC method to determine the drug concentration at each time point. The mean plasma concentration-time curves were plotted. Pharmacokinetic parameters were evaluated using DAS software.

Pharmacodynamic Study

Logarithmically growing A549 cells were trypsinized, washed twice with PBS, and resuspended in sterile PBS at a density of approximately 3×10^7 cells/mL. Under sterile conditions, BALB/c-nu nude mice were selected. The skin of the right anterior axillary region was disinfected with povidone-iodine, and 100 μL of the A549 cell suspension (containing about 3×10^6 cells) was slowly injected subcutaneously using a sterile syringe to establish the NSCLC xenograft tumor model. Tumor volume (V) was calculated using the formula $V = 0.5 \times a \times b^2$, where a and b are the longest and shortest diameters measured with a caliper, respectively. When the tumor volume reached approximately 100 mm^3, tumor-bearing mice were randomly divided into five groups (n=5): (1) Model control group (administered an equal volume of saline), (2) CU group, (3) CU1 group, (4) CU1-LSLN group, and (5) CU1-LCpHL group. All treatment groups received an equivalent CU1 dose of 15 mg/kg via intraperitoneal injection. Administration was performed every other day for a total of 10 doses over 20 days. The model control group received an equal volume of saline on the same schedule. Body weight and tumor volume were measured and recorded regularly during the treatment period.

At the end of the treatment (final tumor volume not exceeding 1000 mm^3, complying with animal ethics requirements), the mice were euthanized by cervical dislocation. Tumors were excised and weighed. The tumor inhibition rate for each group was calculated as follows:

Tumor Inhibition Rate (%) = [(Mean tumor weight of control group - Mean tumor weight of treatment group)/Mean tumor weight of control group] × 100%Subcutaneous tumor tissues and organs (heart, liver, lung, kidney) from each group were collected, rinsed twice with saline, fixed in 4% paraformaldehyde (1:10), and processed for subsequent immunohistochemical (IHC) and hematoxylin-eosin (H&E) staining.

Add 2 mL of rat blood red blood cells (2%) to 98 mL of physiological saline solution and set aside. Take the CU1-LCpHL lyophilized powder and prepare a 1 mg/mL solution. Divide into 8 groups: Group 1: Control group containing only CU1-LCpHL solution without blood Group 2: Complete hemolysis group (positive control) containing equal volume of deionized water without drug solution Group 3: Blank control group (negative control) containing equal volume of physiological saline without drug solution Groups 4–8: Experimental groups containing different concentrations of CU1-LCpHL solution (4%, 8%, 12%, 16%, 20%). All samples were incubated at 37°C for 1h, 3h, and 5h. At each time point, samples were centrifuged (1500 rpm, 10 min), hemolysis was recorded, and the samples were resuspended for continued incubation. Transfer 200 μL of supernatant collected at 5 hours into a 96-well plate. Measure absorbance (A) at 545 nm using an enzyme-linked immunosorbent assay reader. Calculate the hemolysis rate using the following formula: Hemolysis (%) = $(A_{sample} - A_{negative})/(A_{positive} - A_{negative}) \times 100\%$.

Mechanism Validation

Potential targets of CU1 were predicted using the "SwissTargetPrediction" platform. Targets related to NSCLC were retrieved from databases including "DrugBank", "GeneCards", and "OMIM", combined, and deduplicated to obtain a comprehensive target list. The intersection between the predicted drug targets and the NSCLC-related targets was identified. Core targets were analyzed using "Cytoscape 3.8.2" software. Gene Ontology (GO) and Kyoto Encyclopedia of Genes and Genomes (KEGG) pathway enrichment analyses were performed using the "DAVID" platform to predict the mechanism of action of CU1.A549 cells were seeded into 6-well plates. After cell attachment, the medium was replaced with medium containing 25 μM CU1, CU1-LSLN, or CU1-LCpHL, with an untreated blank control group. After 24 h of culture, cellular proteins were extracted for Western blot analysis.

Statistical Analysis

Student's t-tests and ANOVA were used to assess significant differences between two groups and among three groups, respectively, with $P < 0.05$ considered statistically significant.

Results

Optimized Formulation and Characterisation of Long-Circulating pH-Sensitive Nanoliposome of CU1

Initially, this study investigated the impact of DSPE-PEG2000 content on the physicochemical properties of CU1-LCpHL. As shown in Table 1, with increasing the molar ratio of DSPE-PEG2000, both particle size and polydispersity index (PDI) initially decreased, then increased. Concurrently, the encapsulation efficiency (EE%) first increased and then decreased with increasing proportions. Considering particle size, homogeneity, and drug loading efficiency comprehensively, the molar ratio of DOPE: CHEMS: DSPE-PEG2000: CU1 = 6: 4: 0.5: 1 was preliminarily selected to achieve relatively high EE%.

Table 1 Effect of Different Molar Ratios of DSPE-PEG2000 on PDI, Particle Size, and EE (%) ($\bar{x} \pm s$, n = 3)

Molar Ratio (DOPE: CHEMS: DSPE-PEG2000: CU1)	Particle Size (nm)	PDI	EE (%)
6: 4: 0.25: 1	148.4 ± 2.187	0.261 ± 0.004	89.54 ± 2.19
6: 4: 0.5: 1	144.7 ± 2.087	0.243 ± 0.002	90.01 ± 1.08
6: 4: 1: 1	157.1 ± 2.510	0.283 ± 0.021	85.44 ± 3.12

Table 2 Effect of Different Molar Ratios of CU1 on PDI, Particle Size, and EE (%) ($\bar{x} \pm s$, n = 3)

Molar Ratio (DOPE: CHEMS: DSPE-PEG2000: CU1)	Particle Size (nm)	PDI	EE (%)
6: 4: 0.5: 1	144.7 ± 2.087	0.243 ± 0.002	90.01 ± 1.08
6: 4: 0.5: 1.5	147.9 ± 2.843	0.259 ± 0.009	89.39 ± 2.57
6: 4: 0.5: 2	166.5 ± 3.931	0.341 ± 0.017	77.90 ± 2.63

Subsequently, the influence of CU1 loading on liposome quality was further evaluated. As indicated in Table 2, with an increase in the feeding ratio of CU1, both the particle size and PDI of the liposomes increased, while the EE% declined slightly. To achieve a balance between high drug loading and favorable physicochemical properties, the final molar ratio was determined as DOPE: CHEMS: DSPE-PEG2000: CU1 = 6: 4: 0.5: 1.5 and used for subsequent batch preparation.

Based on the optimized formulation and process described above, three batches of CU1-LCpHL samples were prepared in parallel. The lyophilized product appeared as a uniform, bright yellow, loose cake (Figure 1A and B) with good redispersibility, rapidly dispersing in either pure water or 0.9% saline. The resulting liposome dispersion after reconstitution was clear and bright yellow (Figure 1C). Nanoparticle tracking analysis (Figure 1D) revealed a particle size distribution between 50–300 nm, with an average particle size of 125.9 ± 1.65 nm, a PDI of 0.206 ± 0.009, and a Zeta potential of −2.13 ± 0.46 mV (Table 3), indicating uniform particle size and a stable dispersion system. Transmission electron microscopy (TEM) observation (Figure 1E) showed that CU1-LCpHL presented a spherical morphology with uniform particle size distribution and no significant aggregation between particles. The slightly blurred particle edges were speculated to be related to the hydrophilic corona formed by DSPE-PEG2000 on the liposome surface.

In vitro Release Study

The in vitro drug release behavior of free CU1 and CU1-LCpHL was investigated using the dialysis method under simulated physiological (pH 7.4) and tumor-acidic microenvironmental (pH 5.5) conditions. The results are presented in Figure 1F. The cumulative release profiles of free CU1 under both pH conditions nearly overlapped, with no significant difference in the 24-hour cumulative release amount. This indicates that the release behavior of free CU1 is independent of environmental pH, consistent with a simple diffusion-dominated mechanism.

In contrast to the free drug, CU1-LCpHL exhibited distinct sustained-release characteristics. At pH 7.4, the release was slow and steady. However, when the pH of the release medium decreased to 5.5, both the cumulative release amount and release rate of CU1 from CU1-LCpHL were significantly accelerated. These results demonstrate that the constructed CU1-LCpHL possesses pH-dependent release behavior, confirming its acid sensitivity.

Stability Study

The storage stability of CU1-LCpHL dispersion and its lyophilized powder under different conditions was investigated, and the results are shown in Table 4 and Table 5. Freshly prepared CU1-LCpHL dispersion was stored at 4°C and 25°C, respectively. Samples were taken at predetermined intervals to measure particle size, PDI, and encapsulation efficiency (EE%) (Table 4). The data show that, compared to day 0, no significant changes ($P > 0.05$) were observed in particle size, PDI, or EE% for samples stored at 25°C for 7 days or at 4°C for 15 days. This indicates that the quality of CU1-LCpHL dispersion remained stable under the aforementioned conditions and within the specified timeframes.

The long-term stability of CU1-LCpHL lyophilized powder was further evaluated at 25°C (Table 5). Compared with the initially lyophilized product (day 0), key quality attributes of the reconstituted liposomes, including average particle size, PDI, and DL%, remained unchanged after 90 days of storage. These findings suggest that the lyophilization process significantly enhanced the physicochemical stability of CU1-LCpHL, and its lyophilized powder formulation demonstrates promising potential for long-term storage at room temperature.

https://doi.org/10.2147/IJN.S588259

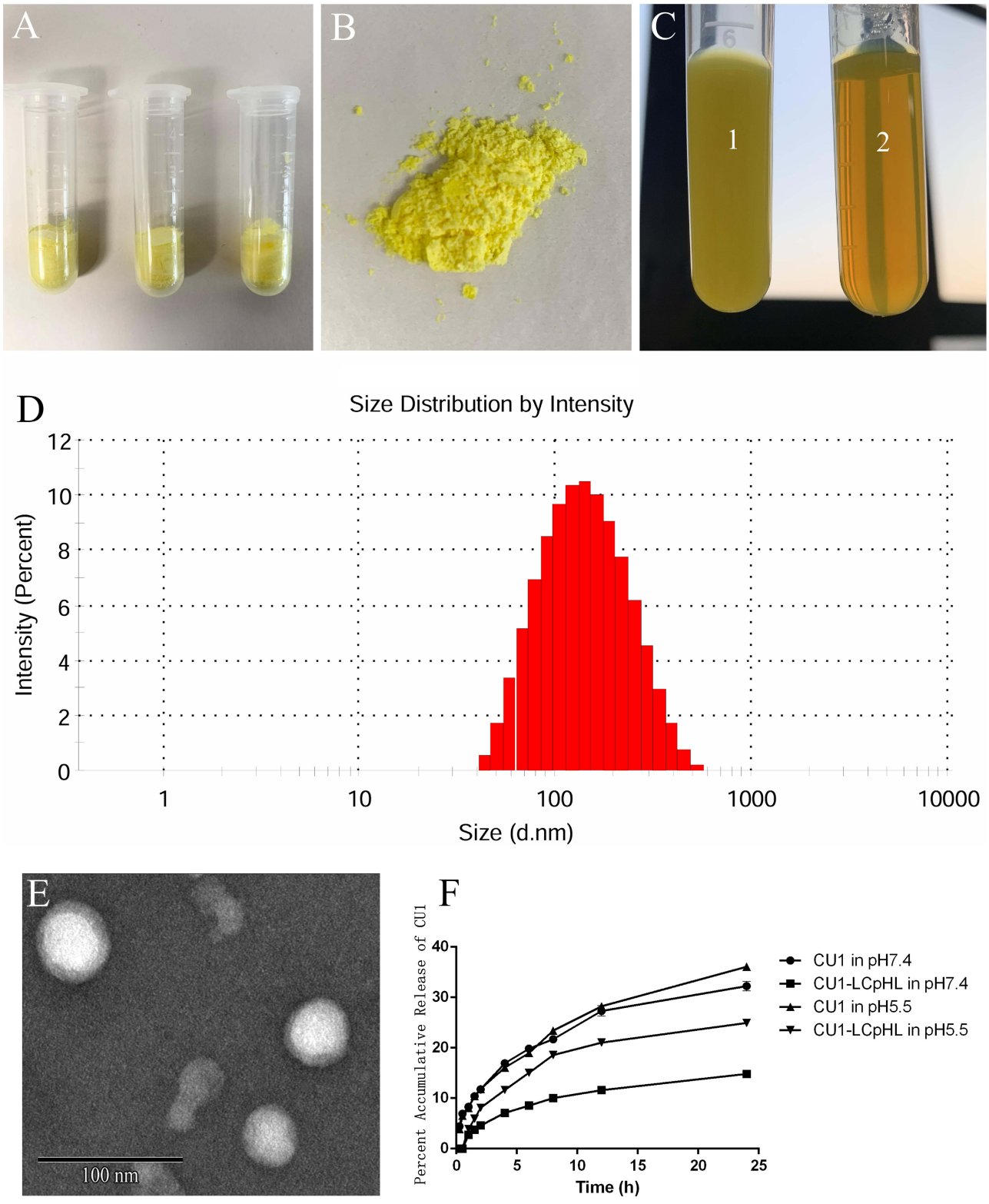

Figure 1 Lyophilized powders (**A** and **B**). Liquid of hydrated CU1-LCpHL ((**C**)-1) and liquid of CU1-LCpHL after sonication ((**C**)-2). The particle size of CU1-LCpHL (**D**), TEM microscopy of CU1-LCpHL (**E**), Cumulative release curves of drugs under different pH conditions (**F**) ($\bar{x} \pm s$, n = 3).

https://doi.org/10.2147/IJN.S588259

Table 3 Verification Test Results of Three Batches of Samples of CU1-LCpHL ($\bar{x} \pm s$, n = 3)

No.	Particle Size (nm)	PDI	Zeta (-mV)	EE (%)	DL (%)
1	127.0 ± 0.764	0.209 ± 0.009	−2.24 ± 0.729	95.07	7.71
2	126.8 ± 0.361	0.208 ± 0.012	−1.85 ± 0.307	94.78	7.61
3	123.8 ± 0.794	0.203 ± 0.008	−2.30 ± 0.163	95.12	7.14
$\bar{x} \pm s$	125.9 ± 1.649	0.206 ± 0.009	−2.13 ± 0.455	94.99 ± 0.18	7.49 ± 0.30

Table 4 The Stability of the Liquid of CU1-LCpHL ($\bar{x} \pm s$, n = 3)

Time	25°C			4°C		
	Particle size (nm)	PDI	EE (%)	Particle size (nm)	PDI	EE (%)
0 d	125.7±0.890	0.210± 0.001	94.13±0.51	125.7±0.890	0.210±0.001	94.13±0.51
1 d	127.8±0.633	0.210±0.036	94.16±0.64	124.2±0.936	0.210±0.033	93.53±0.28
3 d	127.9±1.372	0.209±0.020	93.82±0.72	125.7±0.468	0.201±0.036	93.56±0.87
5 d	126.9±1.648	0.234±0.027	93.88±0.99	126.4±1.241	0.221±0.045	92.63±0.46
7 d	129.7±2.764	0.266±0.042	93.24±0.17	126.2±1.054	0.242±0.002	93.05±0.21
15 d	127.5±2.151	0.285±0.014*	89.59±0.86*	125.6±2.533	0.248±0.048	93.27±0.43
30 d	153.2±3.450*	0.346±0.010*	82.24±0.73*	134.9±2.390*	0.289±0.046	91.69±0.78*
RSD	7.43%	20.42%	4.87%	2.81%	13.26%	0.84%

Note: * $P < 0.05$ compared to 0 d, statistically different.

Table 5 The Stability of the Freeze-Dried Powder of CU1-LCpHL ($\bar{x} \pm s$, n = 3)

Time	Particle Size (nm)	PDI	DL (%)
0 d	132.1 ± 1.090	0.265 ± 0.003	7.51 ± 0.33
3 d	132.4 ± 1.976	0.275 ± 0.012	7.45 ± 0.10
5 d	133.2 ± 0.305	0.261 ± 0.006	7.56 ± 0.21
7 d	131.8 ± 1.598	0.255 ± 0.037	7.24 ± 0.65
15 d	130.5 ± 1.962	0.277 ± 0.025	7.17 ± 0.42
30 d	131.9 ± 0.486	0.280 ± 0.034	7.39 ± 0.59
90 d	134.0 ± 2.551	0.278 ± 0.012	7.21 ± 0.68
90 d RSD	6.58%	4.07%	2.14%

Effects of Long-Circulating pH-Sensitive Nanoliposome of CU1 on Tumor Cells

Cellular Uptake

To evaluate the uptake efficiency of different formulations in tumor cells, a cellular uptake assay was performed using fluorescence labeling. As shown in Figure 2A, after 3 hours of drug treatment, the fluorescence intensity within A549 cells in the CU1-LCpHL-treated group was significantly stronger than that in the CU1-LSLN group, free CU1 group, and CU group. This result indicates that the constructed pH-sensitive liposomes effectively promoted the accumulation and uptake of the drug in the cells.

Cell Apoptosis

The induction of apoptosis in A549 cells by the drugs was detected using flow cytometry with Annexin V-FITC/PI double staining (Figure 2B). The results showed that, at the same concentration, free CU and free CU1 induced a similar degree of apoptosis. The liposomal formulations demonstrated greater apoptosis-inducing activity, with CU1-LCpHL being the most potent. Specifically, the early, late, and total apoptosis rates in the CU1-LSLN group

https://doi.org/10.2147/IJN.S588259

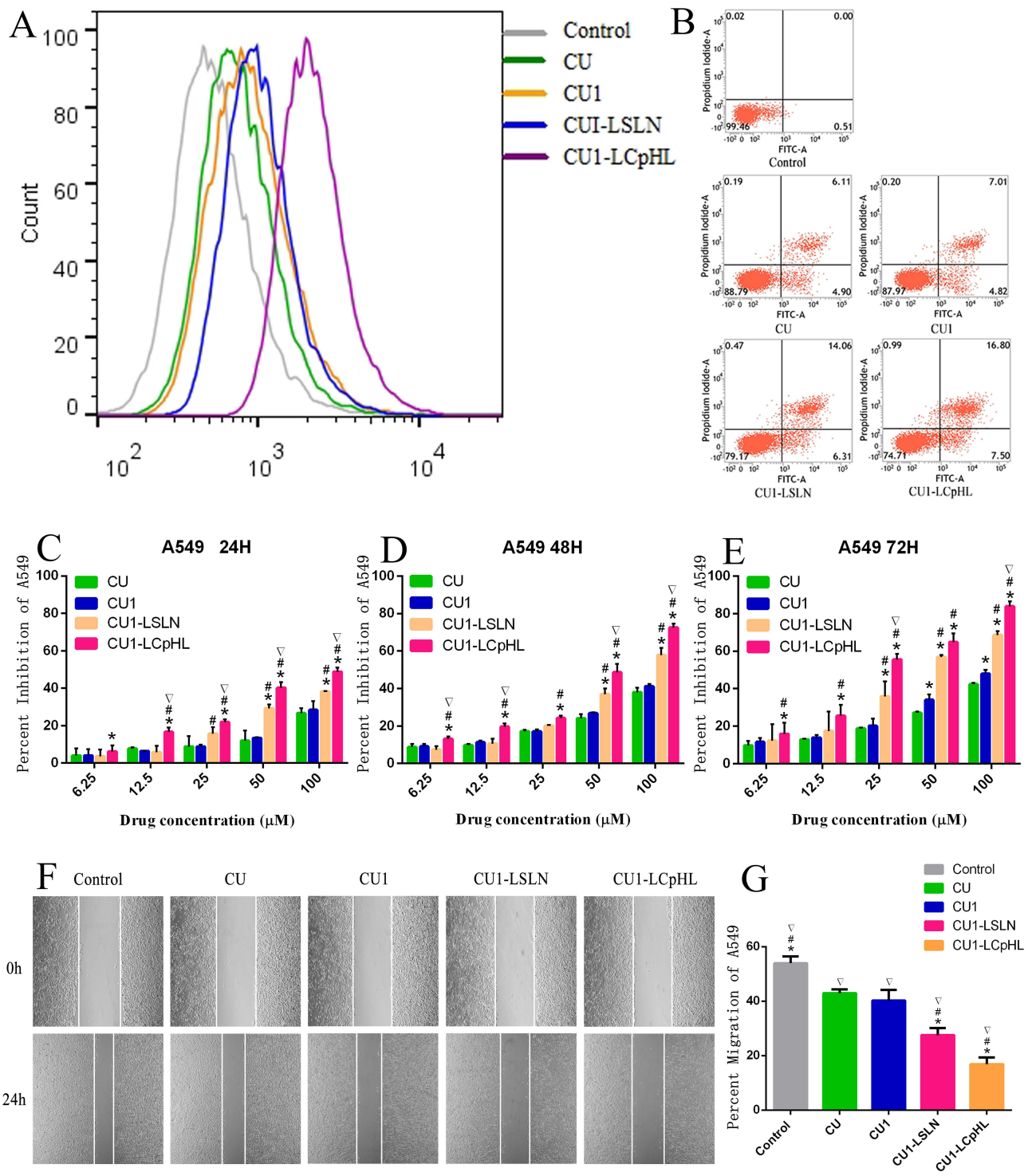

Figure 2 Uptake of CU, CU1, CU1-LSLN, and CU1-LCpHL by A549 cells (**A**). Apoptosis induction of A549 cells by CU, CU1, CU1-LSLN, and CU1-LCpHL for 24 h (**B**). Inhibitory effects of each group on A549 cells at different times ((**C**) 24 h; (**D**) 48 h; (**E**) 72 h) ($\bar{x} \pm s$, n = 3). *$P < 0.05$ compared with CU. #$P < 0.05$ compared with CU1. ∇$P < 0.05$ compared with CU1-LSLN. Migration map (**F**) and mobility (**G**) of A549 cells ($\bar{x} \pm s$, n = 3).

were 6.31%, 14.06%, and 20.37%, respectively. In contrast, for the CU1-LCpHL group, these rates reached 7.50%, 16.80%, and 24.3%, respectively. This enhanced effect may be attributed to CU1-LCpHL's the superior cellular uptake capacity.

Inhibition of Cell Proliferation

The inhibitory effects of different formulations on the proliferation of A549 cells were assessed using the CCK-8 assay (Figure 2C–E). The results demonstrated that at all measured time points (24 h, 48 h, 72 h), the cell proliferation inhibition rate of CU1-LCpHL was significantly higher than that of all other treatment groups ($P < 0.05$), indicating its superior in vitro anti-tumor activity.

Inhibition of Cell Migration

A scratch wound-healing assay was performed to assess the impact of the drugs on A549 cell migration. As shown in Figure 2F and G, 24 hours after drug treatment, the cell migration rate was the lowest in the CU1-LCpHL group. Its ability to inhibit cell migration was significantly stronger than that of all other groups ($P < 0.05$). This is likely due to CU1-LCpHL enhancing drug accumulation within cells and effectively inducing apoptosis, both of which contribute to the suppression of tumor cell migration and invasion.

Pharmacokinetic Study in Rats

Following a single tail vein injection of equivalent doses (15 mg/kg) of CU, CU1, and CU1-LCpHL to SD rats, plasma drug concentrations at various time points were determined, and the plasma concentration-time curves were plotted (Figure 3). Non-compartmental analysis was performed using DAS 2.1.1 software to calculate the main pharmacokinetic parameters (Table 6). The concentration-time curves revealed that CU1-LCpHL was still detectable 1440 minutes post-administration, demonstrating a pronounced long-circulating characteristic.

Compared to free CU1, the pharmacokinetic profile of CU1-LCpHL was significantly improved. The area under the plasma concentration-time curve from zero to infinity ($AUC_{0-\infty}$) for CU1-LCpHL was 24,338.53 μg/L*min, which was 9.47-fold higher than that of the CU1 group. The mean residence time (MRT) and elimination half-life ($t_{1/2}$) were 7.69-fold and 5.89-fold greater, respectively, than those of the CU1 group. Concurrently, the total body clearance (CLz) of CU1-LCpHL was only about 10% of that observed for free CU1.

These results indicate that encapsulating CU1 within pH-sensitive long-circulating liposomes effectively delayed its systemic clearance, significantly increased drug exposure, and prolonged its duration of action, thereby substantially improving its pharmacokinetic properties.

Pharmacodynamic Results

To evaluate the in vivo antitumor efficacy of different formulations, the final volume and weight of subcutaneous xenograft tumors in nude mice were measured. As shown in Figure 4A–C and Table 7: Compared with the control (CU) group, the tumor volume and weight in all treatment groups (CU1, CU1-LSLN, CU1-LCpHL) showed a significant sequential decrease. Quantitative analysis revealed that the CU1-LCpHL group exhibited the most pronounced tumor growth inhibition. Its tumor inhibition rate was 2.42-, 2.17-, and 1.37-fold higher than those of the CU, CU1, and CU1-

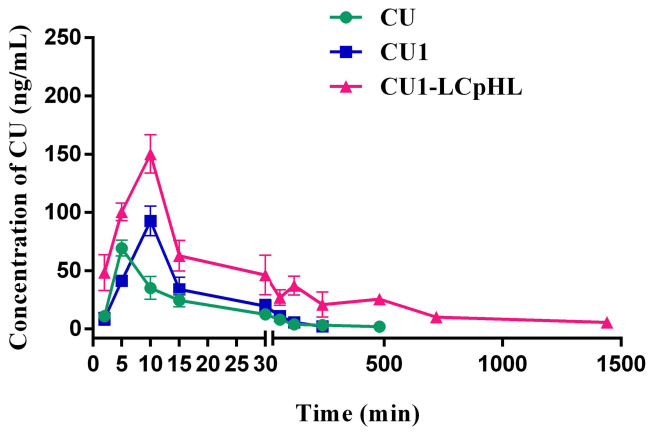

Figure 3 Concentration-time curves ($\bar{x} \pm s$, n = 5).

https://doi.org/10.2147/IJN.S588259

Table 6 The Main Pharmacokinetic Parameters After Giving CU, CU1, or CU1-LCpHL by Tail Vein Injection

Parameter	Unit	CU	CU1	CU1-LCpHL
$AUC_{(0-t)}$	ug/L*min	2557.13	2571.03	24,338.53
$MRT_{(0-t)}$	Min	132.14	57.814	444.982
$t_{1/2z}$	Min	347.62	81.11	477.605
T_{max}	Min	5	10	10
Vz	L/kg	2114.04	619.56	364.50
CLz	L/min/kg	4.21	5.29	0.53
C_{max}	ug/L	69.33	92.68	150.21

LSLN groups, respectively. These results indicate that the acid-sensitive liposomal nano-delivery system, CU1-LCpHL, demonstrated the optimal antitumor efficacy.

To further assess the therapeutic effect from a pathological morphology perspective, hematoxylin and eosin (H&E) staining was performed on the excised tumor tissues. The overall morphology of tumor sections was observed at low magnification (100×) to preliminarily analyze necrotic areas and pathological changes, while detailed cellular morphology was examined at high magnification (400×). As shown in Figure 4D, in the control (CU) group, tumor cells were proliferating vigorously, characterized by large nuclei, high nuclear-to-cytoplasmic ratios, diverse nuclear morphology, dense arrangement, and observable pathological mitotic figures, with no significant necrotic areas. In contrast, tumor tissues from all treatment groups displayed varying degrees of pathological alterations, including nuclear pyknosis, loosely arranged cells, and irregular cell morphology. Notably, the CU1-LCpHL treatment group exhibited the most extensive area of tumor tissue necrosis.

To investigate the systemic safety of CU1-LCpHL, pathological examination via H&E staining was conducted on major organs, including the heart, liver, lung, and kidney of the nude mice. As shown in Figure 4E, no obvious pathological changes were observed in the heart, lung, or kidney tissues of animals from any group. In liver tissues, the control group showed inflammatory cell infiltration and signs of suspected tumor cell metastasis, with some hepatocytes exhibiting unclear morphological structure. In the CU and CU1 groups, some hepatocytes displayed nuclear enlargement and irregular nuclear morphology. In contrast, the liver tissues in the CU1-LSLN and CU1-LCpHL groups showed largely normal histopathology: liver lobule architecture was intact, and the morphology of most hepatocytes was normal. This indicates that the CU1-LCpHL nano-delivery system, while exerting potent antitumor effects, did not cause significant damage to major organs, demonstrating favorable biosafety.

Hemocompatibility is the primary safety evaluation indicator for intravenous nanoparticle formulations. Figure 4F shows that the pure CU1-LCpHL solution without red blood cell suspension (Group 1) appears clear, transparent, and bright yellow. The positive control group (Group 2) exhibits complete hemolysis with a distinct red color, while the negative control group (Group 3) remains colorless with no hemolysis observed. No significant hemolysis was detected in the other experimental groups. As shown in Figure 4G, at a CU1-LCpHL concentration of 0.8 mg/mL, the hemolysis rate was only 2.95%, below 5%, indicating good safety. In the high-concentration group, even at 1 mg/mL CU1-LCpHL, the hemolysis rate remained at 5.70%. These results suggest that CU1-LCpHL does not cause severe hemolysis and is relatively safe.

Mechanism Validation

To investigate the potential molecular mechanisms of CU1 against non-small cell lung cancer (NSCLC), the intersection between predicted drug targets and NSCLC disease targets was first obtained, yielding 61 common targets (Figure 5A). This target set was imported into the STRING database to construct a protein-protein interaction (PPI) network. Analysis using Cytoscape software identified 10 core targets. Ranked in descending order by degree value (Degree), they were AKT, TNF, Caspase-3, EP300, mTOR, etc. (Figure 5B). Gene Ontology (GO) functional annotation and Kyoto Encyclopedia of Genes and Genomes (KEGG) pathway enrichment analyses were further performed on the common

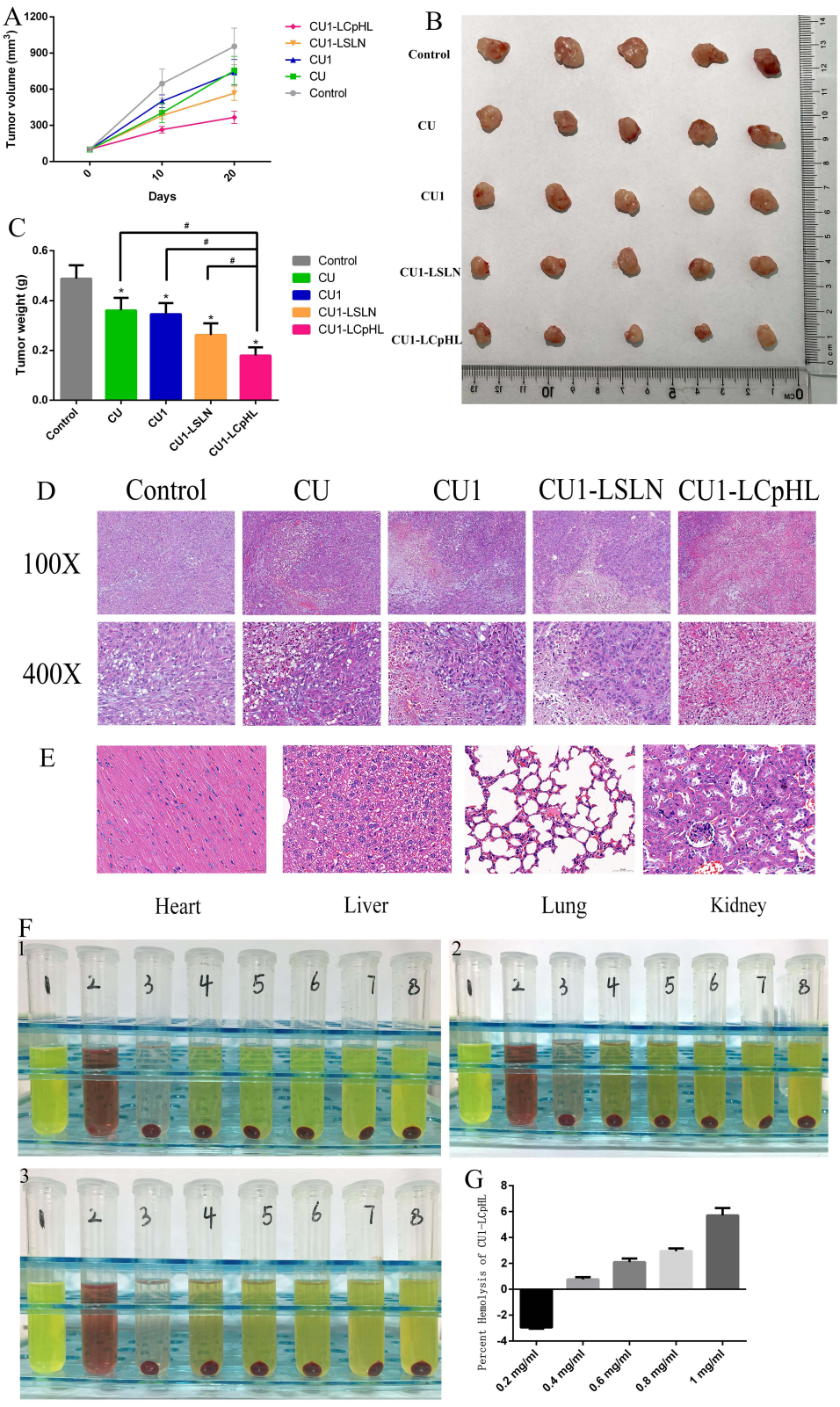

Figure 4 Volume change of subcutaneous xenograft tumor (**A**). Tumor entity diagram (**B**). Difference of tumor weight in each group (n = 5) (**C**). * Compared with control, $P < 0.05$. # Compared with CU1-LCpHL, $P < 0.05$. HE staining of subcutaneous xenografts in nude mice (**D**) and pathological sections of heart, liver, lung, and kidney tissues in tumor-bearing mice. (400X) (**E**). The hemolysis of CU1-LCpHL at different time points (1: 1 h; 2: 3 h; 3: 5 h) (**F**). Hemolysis rate of CU1-LCpHL (**G**).

https://doi.org/10.2147/IJN.S588259

Table 7 Weight of Subcutaneous Xenografts and Tumor Inhibition Rate ($\bar{x} \pm s$, n = 5)

	Control	CU	CU1	CU1-LSLN	CU1-LCpHL
Tumor weight (g)	0.49 ± 0.05	0.36 ± 0.05	0.35 ± 0.04	0.26 ± 0.05	0.18 ± 0.03
Inhibitory tumor rate (%)	–	26.21 ± 5.07	29.19 ±4.41	46.39 ± 4.73	63.36 ± 3.34

targets using the DAVID platform. The GO analysis results (Figure 5C) indicated significant enrichment for 100 terms across biological processes, molecular functions, and cellular components. The KEGG pathway analysis (Figure 5D) suggested that pathways, including pathways in cancer, hepatitis B, TNF signaling, and T cell receptor signaling, might primarily mediate the anticancer effects of CU1.

To validate the above bioinformatics predictions and explore the mechanism underlying the enhanced efficacy of CU1-LCpHL, the expression levels of key apoptosis-related proteins were examined using Western blot analysis. The results (Figure 5E) showed that, compared to the free CU1 group, treatment with CU1-LCpHL significantly upregulated

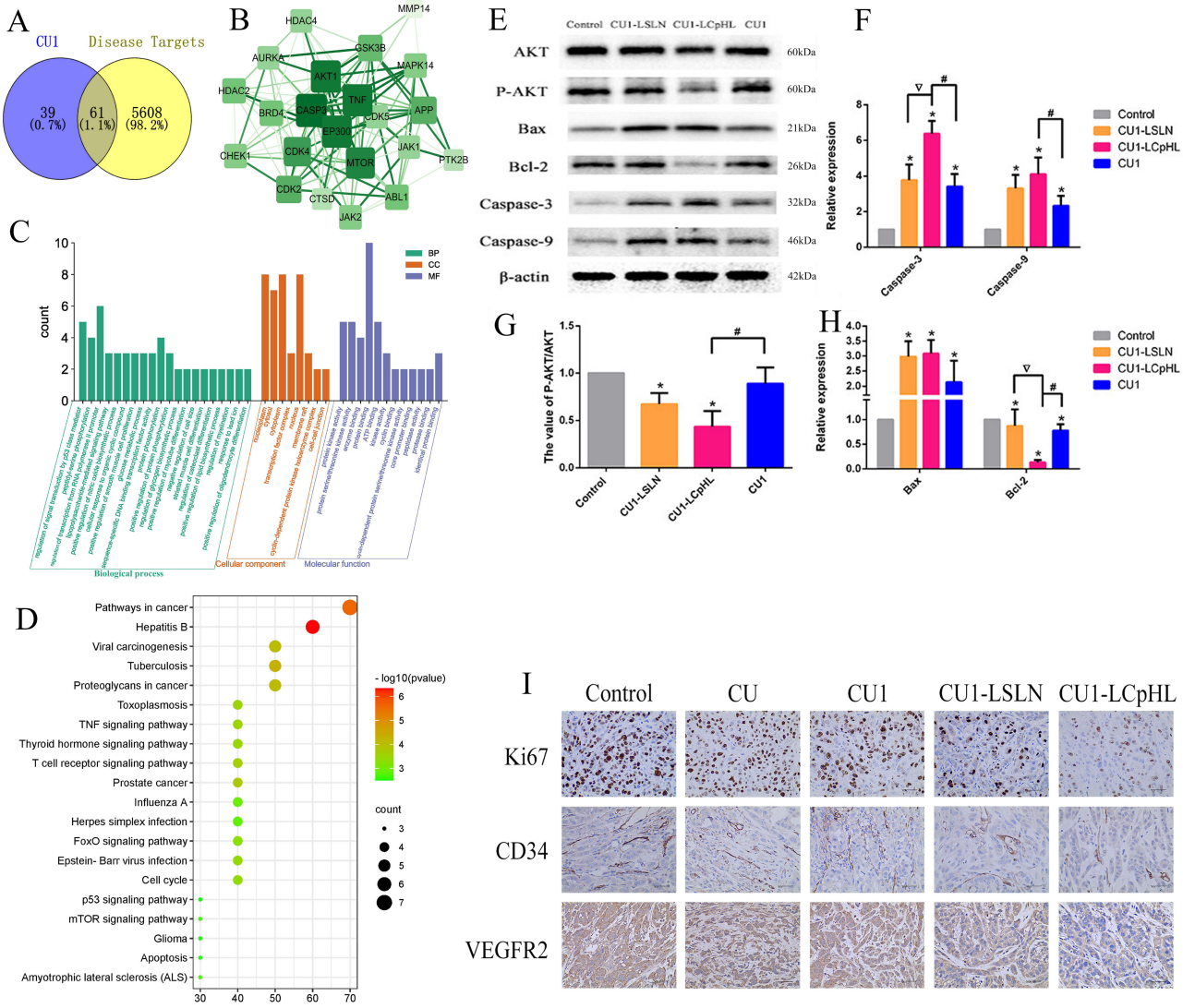

Figure 5 (**A**) Venn diagram of the shared targets of CU1 and non-small cell lung carcinoma. (**B**) Protein-interactive (PPI) network based on the targets for CU1 in the treatment of non-small cell lung carcinoma. (**C**) GO enrichment analysis of the hub targets for CU1 in the treatment of non-small cell lung carcinoma. (**D**) The 20 KEGG pathways enriched for hub targets in CU1 for the treatment of non-small cell lung carcinoma. Western Blot image (**E**); Relative grayscale analysis of Caspase-3 and Caspase-3 proteins (**F**); Relative ratio analysis of P-AKT/AKT (**G**); Relative grayscale analysis of Bax and Bcl-2 proteins (**H**). *Compared with the Control group, $P < 0.05$. # Compared with the CU1 group, $P < 0.05$. ▽ Compared with the CU1-LSLN group, $P < 0.05$. Immunohistochemical analysis of subcutaneous xenografts in nude mice (400X) (**I**).

the expression levels of the pro-apoptotic proteins Caspase-3 and Caspase-9 ($P < 0.05$) (Figure 5F), and significantly downregulated the expression levels of the P-AKT/AKT ($P < 0.05$) (Figure 5G). Concurrently, the expression of Caspase-3 in the CU1-LCpHL group was also significantly higher than that in the CU1-LSLN group. Furthermore, the expression level of the anti-apoptotic protein Bcl-2 in the CU1-LCpHL group was significantly lower than that in both the CU1 and CU1-LSLN groups ($P < 0.05$) (Figure 5H). These results indicate that CU1-LCpHL activates the apoptotic pathway more effectively in lung cancer cells.

To evaluate the inhibitory effects of different formulations on tumor proliferation and angiogenesis, the expression of the proliferation marker Ki67, the vascular endothelial marker CD34, and vascular endothelial growth factor receptor 2 (VEGFR2) in tumor tissues was assessed via immunohistochemistry (IHC). The results (Figure 5I) revealed a consistent decreasing trend in the positive expression rates of Ki67, CD34, and VEGFR2: CU1-LCpHL group < CU1-LSLN group < CU1 group < CU group. This demonstrates that following CU1-LCpHL treatment, tumor cell proliferative activity and microvascular generation were most significantly suppressed.

Discussion

Curcumin (CU) has garnered significant attention due to its broad-spectrum anti-tumor activity. However, its inherent limitations, including instability, poor aqueous solubility, and low bioavailability, severely restrict its clinical application.[10–12] To overcome these bottlenecks, our research team previously modified its phenolic hydroxyl groups, successfully obtaining the derivative CU1. This compound maintained anti-proliferative activity against lung cancer cells comparable to CU while exhibiting significantly improved chemical stability.[13] Nevertheless, CU1 still faces challenges related to poor water solubility and low in vivo bioavailability. To address this, this study designed and constructed an acid-sensitive long-circulating liposomal nano-delivery system (CU1-LCpHL). The aim was to exploit the acidic tumor microenvironment for targeted drug release and to prolong its systemic circulation time via polyethylene glycol (PEG) modification, thereby ultimately enhancing the anti-lung cancer efficacy of CU1.

In pharmaceutical formulation studies, formulation optimization is crucial for ensuring nanoparticle performance. We found that the amount of the long-circulating material DSPE-PEG2000 significantly impacted the drug encapsulation efficiency (EE%), showing an initial increase followed by a decrease with higher amounts. This is likely because an appropriate amount of DSPE-PEG2000 helps form a stable lipid bilayer for drug encapsulation. In contrast, excess DSPE-PEG2000 can form micelle- or gel-like structures, hindering effective drug encapsulation, as reported previously.[32,33] After embedding a small amount of PEG chains into the liposome membrane, hydrophobic interactions and electrostatic forces at the particle surface are reduced, preventing liposomes from aggregating into larger particles. Simultaneously, the steric hindrance of PEG chains facilitates more uniform dispersion of liposome particles during hydration, resulting in a concurrent decrease in PDI.[34] Excessive hydrophobic ends (DSPE) of DSPE-PEG2000 displace DOPE and CHEMS, disrupting the complementary bilayer structure they form. This compromises membrane integrity, making particles prone to fusion. Excessive PEG chains intertwine on the membrane surface, forming localized "gel layers" that increase indirect interactions between particles. This induces mild aggregation, ultimately manifesting as increased liposome size and an uneven size distribution.[35] Consequently, we determined the optimal formulation with a molar ratio of DOPE: CHEMS: DSPE-PEG2000: CU1 = 6:4:0.5:1.5. Stability studies indicated a limited shelf life for the liquid CU1-LCpHL dispersion, whereas the lyophilized formulation prepared via freeze-drying remained stable for at least 3 months at 25 °C, significantly improving its feasibility for clinical application. In vitro release studies confirmed the pronounced pH-dependent drug release behavior of CU1-LCpHL, with both cumulative release (25.36%) and release rate being significantly higher under acidic conditions (pH 5.0) than under neutral conditions (pH 7.4) (15.02%). The mechanism involves protonation of CHEMS in an acidic environment, disrupting its spatial complementarity with DOPE and destabilizing the lipid bilayer, thereby triggering rapid drug release.[22–24] This characteristic aligns with the micro-environment's acidic nature, laying the foundation for targeted drug release at the tumor site. Further cell experiments demonstrated that this acid-responsive release property facilitated the uptake of CU1-LCpHL by tumor cells. Its uptake efficiency within a short period was significantly higher than that of conventional liposomes (CU1-LSLN), resulting in stronger effects on inducing apoptosis, inhibiting proliferation, and suppressing migration.

 https://doi.org/10.2147/IJN.S588259

Pharmacokinetic studies confirmed the superiority of CU1-LCpHL in vivo. Compared to free CU1, CU1-LCpHL significantly improved drug bioavailability, prolonged the mean residence time and half-life in vivo, and substantially reduced the clearance rate. This improvement is primarily attributed to the PEG modification on the liposome surface. The PEG chains, through steric hindrance and the formation of a hydrophilic corona, effectively prevent the nanoparticles from being rapidly recognized and cleared by the reticuloendothelial system (RES), achieving a long-circulating effect.[34–37] The extended blood circulation time allows CU1-LCpHL to accumulate more in tumor tissue via the enhanced permeability and retention (EPR) effect of solid tumors. Combined with its acid-triggered release mechanism, this ultimately achieves and sustains a higher drug concentration at the target site.

In vivo anti-tumor experiments strongly validated the therapeutic advantage of CU1-LCpHL. First, we optimized the administration solvent, replacing a previously irritating formulation with a mixture of PEG400 and normal saline to ensure the safety of animal experiments.[38] The in vivo efficacy evaluation showed that the CU1-LCpHL group exhibited the greatest tumor inhibition, with a tumor inhibition rate significantly higher than that of the CU1 and CU1-LSLN groups. This confirms the advantage of the acid-sensitive liposome design in utilizing the tumor microenvironment for passive targeting and controlled release. Importantly, histopathological analysis of major organs indicated that CU1-LCpHL did not cause significant cardiac, pulmonary, or renal toxicity. Furthermore, no significant pathological damage or signs of tumor metastasis were observed in liver tissue, nor was there any evident hemolysis, indicating its excellent biological safety.

To further investigate the molecular mechanisms underlying the enhanced anti-tumor effect of CU1-LCpHL, we conducted a study integrating network pharmacology predictions with experimental validation. Network pharmacology analysis suggested that the anti-lung cancer effect of CU1 might involve multiple pathways, including AKT, Caspase-3, and TNF. Subsequent Western blot experiments confirmed that CU1-LCpHL could more effectively modulate key apoptosis-related proteins: significantly upregulating the expression of pro-apoptotic proteins Caspase-3 and Caspase-9, while downregulating the anti-apoptotic protein Bcl-2. Additionally, it significantly reduced AKT phosphorylation. AKT is a critical signaling node regulating cell survival and proliferation, and inhibition of its activation can further promote apoptosis.[39] These results indicate that CU1-LCpHL not only delivers the drug efficiently but also amplifies CU1's pro-apoptotic effect by strengthening inhibition of the AKT signaling pathway and activating the intrinsic apoptotic pathway. Immunohistochemistry results further revealed that CU1-LCpHL exerted the strongest inhibitory effect on the expression of the tumor proliferation marker Ki67, the vascular endothelial marker CD34, and vascular endothelial growth factor receptor 2 (VEGFR2), indicating its comprehensive advantage in inhibiting tumor cell proliferation and angiogenesis.[40–42]

Conclusion

This study successfully developed a novel acid-sensitive, long-circulating liposome, CU1-LCpHL. This drug delivery system prolongs circulation via polyethylene glycol modification, targets tumor tissues via the EPR effect, and triggers rapid drug release in the acidic tumor microenvironment, thereby significantly enhancing CU1 accumulation and utilization efficiency at tumor sites. To advance the next phase of new drug development, this study proposes a 6-month stability test as a follow-up, supplemented by long-term experiments to support the commercial prospects of this formulation. This work provides a highly promising nanodelivery strategy for enhancing the drugability of copper and its derivatives, laying the foundation for subsequent clinical translation studies.

Data Sharing Statement

If needed, data may be requested from the corresponding author.

Ethics Approval and Consent to Participate

The animal studies were conducted in compliance with Southwest Medical University's institutional animal care regulations and guidelines, and adhered to the ARRIVE guidelines. All animal experiments were approved (No. 2020335) by the Ethics Committee of Southwest Medical University.

Author Contributions

All authors made a significant contribution to the work reported, whether that is in the conception, study design, execution, acquisition of data, analysis and interpretation, or in all these areas; took part in drafting, revising or critically reviewing the article; gave final approval of the version to be published; have agreed on the journal to which the article has been submitted; and agree to be accountable for all aspects of the work.

Funding

This study was supported by the National Natural Science Foundation of China (No.82474105), the Major Scientific Research Project of Sichuan Provincial Administration of Traditional Chinese Medicine for the 2025 Special Funds for Traditional Chinese Medicine (No. 25ZDAZX006), Sichuan Provincial Natural Science Foundation Project (No.2024NSFSC0049), the Science and Technology Strategic Cooperation Programs of Luzhou Municipal People's Government and Southwest Medical University (2024LZXNYDJ009).

Disclosure

The authors declare no conflicts of interest in this work.

References

1. Cortes J, Perez-García JM, Llombart-Cussac A, et al. Enhancing global access to cancer medicines. CA Cancer J Clin. 2020;70(2):105–124. doi:10.3322/caac.21597
2. Bray F, Laversanne M, Sung H, et al. Global cancer statistics 2022: GLOBOCAN estimates of incidence and mortality worldwide for 36 cancers in 185 countries. CA Cancer J Clin. 2024;74(3):229–263. doi:10.3322/caac.21834
3. Feng T, Wei Y, Lee RJ, Zhao L. Liposomal curcumin and its application in cancer. Int J Nanomed. 2017;12:6027–6044. doi:10.2147/IJN.S132434
4. Di Maio M, Basch E, Bryce J, Perrone F. Patient-reported outcomes in the evaluation of toxicity of anticancer treatments. Nat Rev Clin Oncol. 2016;13(5):319–325. doi:10.1038/nrclinonc.2015.222
5. Twelves C, Jove M, Gombos A, Awada A. Cytotoxic chemotherapy: still the mainstay of clinical practice for all subtypes metastatic breast cancer. Crit Rev Oncol Hematol. 2016;100:74–87. doi:10.1016/j.critrevonc.2016.01.021
6. Wu XF, Shi L, Zhang S. Research progress of natural anticancer drugs. J Logist Univ PAP Med Sci. 2016;(9):769–772.
7. Bi WJ, Mu XJ, Abulimite ZLPY, Li QD. Progress in Targeting-Delivery Systems for Curcumin. Chin Pharm J. 2015;50(4):323–329.
8. Kunnumakkara AB, Anand P, Aggarwal BB. Curcumin inhibits proliferation, invasion, angiogenesis and metastasis of different cancers through interaction with multiple cell signaling proteins. Cancer Lett. 2008;269(2):199–225. doi:10.1016/j.canlet.2008.03.009
9. Cheng AL, Hsu CH, Lin JK, et al. Phase I clinical trial of curcumin, a chemopreventive agent, in patients with high-risk or pre-malignant lesions. Anticancer Res. 2001;21(4B):2895–2900.
10. Liu J, Huang YH, Wang BH, Liu CX. Research progress on the metabolic pathways in vivo and their metabolites of curcuminoids. Drugs Clinic. 2015;30(12):1553–1557.
11. Peng S, Li Z, Zou L, et al. McClements, Enhancement of curcumin bioavailability by encapsulation in sophorolipid-coated nanoparticles: an in vitro and in vivo study. J Agric Food Chem. 2018;66(6):1488–1497. doi:10.1021/acs.jafc.7b05478
12. Zhao S, Pi C, Ye Y, et al. Recent advances of analogues of curcumin for treatment of cancer. Eur J Med Chem. 2019;180:524–535. doi:10.1016/j.ejmech.2019.07.034
13. Li K, Pi C, Wen J, et al. Formulation of the novel structure curcumin derivative-loaded solid lipid nanoparticles: synthesis, optimization, characterization and anti-tumor activity screening in vitro. Drug Deliv. 2022;29(1):2044–2057. doi:10.1080/10717544.2022.2092235
14. Reyes-Castellanos G, Masoud R, Carrier A. Mitochondrial Metabolism in PDAC: from Better Knowledge to New Targeting Strategies. Biomedicines. 2020;8(8):270. doi:10.3390/biomedicines8080270
15. Chen L, Gao W. Formation mechanism of tumor acidic microenvironment and its effects on tumor progression. Tumor. 2019;39(2):140–145.
16. Zhang HL, Zhu DD, Lin ST, Cai GL, Li N, Liu XX. Advance in the application of acid-sensitive drug delivery system in cancer therapy. Cent South Pharm. 2019;17(12):2091–2099.
17. Kato Y, Ozawa S, Miyamoto C, et al. Acidic extracellular microenvironment and cancer. Cancer Cell Int. 2013;13(1):89–96. doi:10.1186/1475-2867-13-89
18. Zheng X, Yang H, Zhang Z, et al. pH-responsive size-adjustable liposomes induce apoptosis of fibroblasts and macrophages for rheumatoid arthritis treatment. Acta Biomater. 2024;179:256–271. doi:10.1016/j.actbio.2024.03.006
19. Xia J, Chen C, Dong M, et al. Ginsenoside Rg3 endows liposomes with prolonged blood circulation and reduced accelerated blood clearance. J Control Release. 2023;364:23–36. doi:10.1016/j.jconrel.2023.10.023
20. Liu G, Zhao X, Zhang Y, et al. Engineering Biomimetic Platesomes for pH-Responsive Drug Delivery and Enhanced Antitumor Activity. Adv Mater. 2019;31(32):1900795.1–1900795.12. doi:10.1002/adma.201900795
21. Li Y, Zhai Y, Liu W, et al. Ultrasmall nanostructured drug based pH-sensitive liposome for effective treatment of drug-resistant tumor. J Nanobiotechnology. 2019;17(1):117–130. doi:10.1186/s12951-019-0550-7
22. Chang J, Qiao MX, Zhao XL, Hu HY, Chen DW. Formulation optimization and characterization of paditaxe-loaded pH-sensitive liposomes modified with tocopheryl polyethylene glycol 1000 succinate. J Shenyang Pharm Univ. 2017;3:213–220.
23. Kanamala M, Wilson WR, Yang M, Palmer BD, Wu Z. Mechanisms and biomaterials in pH-responsive tumour targeted drug delivery: a review. Biomaterials. 2016;85:152–167. doi:10.1016/j.biomaterials.2016.01.061

24. Khan A, Aljarbou AN, Aldebasi YH, et al. Fatty Acid Synthase (FASN) siRNA-Encapsulated-Her-2 Targeted Fab'-Immunoliposomes for Gene Silencing in Breast Cancer Cells. Int J Nanomed. 2020;15:5575–5589. doi:10.2147/IJN.S256022
25. Wei Y, Li K, Zhao W, et al. The Effects of a Novel Curcumin Derivative Loaded Long-Circulating Solid Lipid Nanoparticle on the MHCC-97H Liver Cancer Cells and Pharmacokinetic Behavior. Int J Nanomed. 2022;17:2225–2241. doi:10.2147/IJN.S363237
26. Carvalho Júnior AD, Vieira FP, Melo VJ, et al. Preparation and cytotoxicity of cisplatin-containing liposomes. Braz J Med Biol Res. 2007;40 (8):1149–1157. doi:10.1590/S0100-879X2006005000125
27. de Oliveira Silva J, Fernandes RS, Ramos Oda CM, et al. Folate-coated, long-circulating and pH-sensitive liposomes enhance doxorubicin antitumor effect in a breast cancer animal model. Biomed Pharmacother. 2019;118:109323. doi:10.1016/j.biopha.2019.109323
28. Feng X, Pi C, Fu S, et al. Combination of curcumin and paclitaxel liposomes exhibits enhanced cytotoxicity towards A549/A549-T cells and unaltered pharmacokinetics. J Biomed Nanotechnol. 2020;16(8):1304–1313. doi:10.1166/jbn.2020.2969
29. Chen Y, Zhang L, Yang Z, Yu J. Curcumin inhibits cerebral ischaemia-reperfusion injury and cell apoptosis in rats through the ERK-CHOP-caspase -11 pathway. Pharm Biol. 2022;60(1):854–861. doi:10.1080/13880209.2022.2069271
30. Freichel T, Heine V, Laaf D, et al. Sequence-Defined Heteromultivalent Precision Glycomacromolecules Bearing Sulfonated/Sulfated Nonglycosidic Moieties Preferentially Bind Galectin-3 and Delay Wound Healing of a Galectin-3 Positive Tumor Cell Line in an In Vitro Wound Scratch Assay. Macromol Biosci. 2020;20(9):e2000163. doi:10.1002/mabi.202000163
31. Yang SS, Ma S, Dou H, et al. Breast cancer-derived exosomes regulate cell invasion and metastasis in breast cancer via miR-146a to activate cancer associated fibroblasts in tumor microenvironment. Exp Cell Res. 2020;391(2):111983. doi:10.1016/j.yexcr.2020.111983
32. Sun DN, Wu Y, Niu L, Jin YH, Chen DW. Preparation of curcumin long-cycle solid lipid nanoparticles and their physicochemical properties. Dep Chin J Pharm. 2011;6:105–112.
33. Sahoo RK, Kumar H, Jain V, Sinha S, Ajazuddin G. Studies on PEGylated and drug-loaded PAMAM dendrimers. J Bioact Compat Polym. 2005;20 (1):113–128. doi:10.1177/0883911505049656
34. Vonarbourg A, Passirani C, Saulnier P, Benoit JP. Parameters influencing the stealthiness of colloidal drug delivery systems. Biomaterials. 2006;27 (24):4356–4373. doi:10.1016/j.biomaterials.2006.03.039
35. Otsuka H, Nagasaki Y, Kataoka K. PEGylated nanoparticles for biological and pharmaceutical applications. Adv Drug Deliv Rev. 2003;55 (3):403–419. doi:10.1016/S0169-409X(02)00226-0
36. Sun DN. In vivo pharmacokinetic study of curcumin long-circulating solid lipid nanoparticles in rats. Chin J Mod Appl Pharm. 2014;8(9):226–227.
37. Fundarò A, Cavalli R, Bargoni A, Vighetto D, Zara GP, Gasco MR. Non-stealth and stealth solid lipid nanoparticles (SLN) carrying doxorubicin: pharmacokinetics and tissue distribution after i.v. administration to rats. Pharmacol Res. 2000;42(4):337–343. doi:10.1006/phrs.2000.0695
38. Barbosa MV, Monteiro LO, Carneiro G, et al. Experimental design of a liposomal lipid system: a potential strategy for paclitaxel-based breast cancer treatment. Colloids Surf B Biointerfaces. 2015;136:553–561. doi:10.1016/j.colsurfb.2015.09.055
39. Romorini L, Garate X, Neiman G, et al. AKT/GSK3β signaling pathway is critically involved in human pluripotent stem cell survival. Sci Rep. 2016;6(1):35660. doi:10.1038/srep35660
40. Lu F, Li K, Wu R, et al. Time-dependent diffusion MRI derived microstructure parameters to predict differentiation degree and Ki-67 expression in rectal cancer. Eur J Radiol. 2025;195:112522. doi:10.1016/j.ejrad.2025.112522
41. Batur S, Ozcan K, Ozcan G, et al. Superficial CD 34 positive fibroblastic tumor: report of three cases and review of the literature. Int J Dermatol. 2019;58(4):416–422. doi:10.1111/ijd.14357
42. Zhang Q, Lu S, Li T, et al. ACE2 inhibits breast cancer angiogenesis via suppressing the VEGFa/VEGFR2/ERK pathway. J Exp Clin Cancer Res. 2019;38(1):173. doi:10.1186/s13046-019-1156-5